# Recent Contributions to Experiments on Cylindrical Shell Panel Flutter

W. HORN*
*Corps of Army Engineers, Vicksburg, Miss.*
AND
G. BARR†
*Sandia Laboratories, Albuquerque, N.Mex.*
AND
L. CARTER‡
*University of Missouri, Kansas City, Mo.*
AND
R. STEARMAN§
*The University of Texas, Austin, Texas*

**Experimental studies have been carried out on the aeroelastic stability of several cylindrical shell configurations under various internal stress levels and supersonic flow conditions. These experiments were conducted in the AEDC Propulsion Wind Tunnel Facility over the Mach number range 1.2–3.5. They demonstrated that the still-air buckling characteristics of thin cylindrical shells were not significantly influenced by the supersonic airstream. In addition, two basic types of panel flutter instabilities were found. One was of a mild limited amplitude motion which resulted in no apparent damage to the shell even though it persisted for several minutes. The second type of panel flutter encountered was more highly divergent or explosive in character destroying the shell within a few seconds after its onset. The nature of these two types of panel flutter instabilities were found to be closely linked to the fluid boundary-layer characteristics.**

## Nomenclature

$BLC$ = boundary-layer control
$C_F$ = mean or total skin-friction coefficient averaged over length $x$ of model
$C_P$ = pressure coefficient
$E$ = Young's modulus of elasticity
$F(y/\delta)$ = velocity defect function
$F(\eta)$ = law of the wall function
$g$ = acceleration due to gravity
$h$ = shell thickness
$L$ = shell length
$M_1, M_\infty$ = freestream Mach number
$\bar{N}_x$ = applied axial stress resultant
$\tilde{N}_x$ = buckling load ratio, $\bar{N}_x R[3(1-\nu^2)]^{1/2}/Eh^2$
$P$ = net axial compressive loading
$\bar{p}$ = pressure differential across shell skin, positive for tensile hoop stress, psig
$\tilde{p}$ = buckling pressure ratio, $\bar{p}/E(R/h)^2[12(1-\nu^2)^{1/2}/\pi^2]$
$P_{T_1}, P_{T_\infty}$ = freestream total pressure
$R$ = shell radius
$R_e$ = Reynolds number
$U^*$ = friction velocity
$U, U_1, U_\infty$ = freestream velocity
$U_\delta$ = velocity at outer edge of boundary layer
$\dot{w}$ = weight flow injected $BLC \sim$ lb/sec
$x$ = distance along model axis
$y$ = radial distance measured in direction of outer normal to model surface
$\alpha_o$ = ogive model angle of attack
$\delta$ = boundary-layer thickness
$\delta_1$ = boundary-layer displacement thickness
$\eta$ = law of the wall parameter, $yU^*/\nu_w$
$\theta$ = boundary-layer momentum thickness
$\lambda$ = BLC mass injection parameter, $\dot{w}/g\rho_1 U_1$
$\nu$ = Poisson's ratio
$\nu_w$ = kinematic viscosity at model surface
$\rho_1$ = freestream fluid mass density

Presented as Paper 71-328 at the AIAA/ASME 12th Structures, Structural Dynamics and Materials Conference, Anaheim, Calif., April 19–21, 1971; submitted August 28, 1973; revision received May 3, 1974. This research was supported by the Air Force Office of Scientific Research, Office of Aerospace Research, U.S. Air Force, and the Arnold Engineering Development Center Propulsion Wind Tunnel Facility, U.S. Air Force.

Index categories: Aeroelasticity and Hydroelasticity; Aircraft Configuration Design; Optimal Structural Design.

* Aerospace Engineer, Waterways Experiment Station.
† Staff Member.
‡ Graduate Student.
§ Professor, Department of Aerospace Engineering and Engineering Mechanics. Member AIAA.

## Introduction

THE complex problems of panel flutter and divergence, and panel response due to aerodynamic noise and turbulence is one of practical consideration in the design of skin panels on aerospace vehicles, and high-performance aircraft and missiles. Although preliminary aeroelastic design criteria have evolved to a fair degree for the flat panel elements, very little design information has appeared for thin shell-type structures. A general survey of this problem and a limited amount of design information for shells can be found in Refs. 1–18.

The lack of available aeroelastic and more specifically panel flutter design criteria on thin shell structures was the result of several practical considerations. The earlier experimental studies, for example, indicated that the existing theoretical predictions concerning panel flutter of cylindrical shells were conservative and shell structures were much less prone to panel flutter than originally indicated by theory. Furthermore, if panel flutter did occur it appeared to be a mild limited amplitude motion which resulted in no apparent damage to the structure. It, therefore, was not considered to be a serious threat to the structural integrity of existing rocket and missile designs for the short time that they would be exposed to environmental conditions

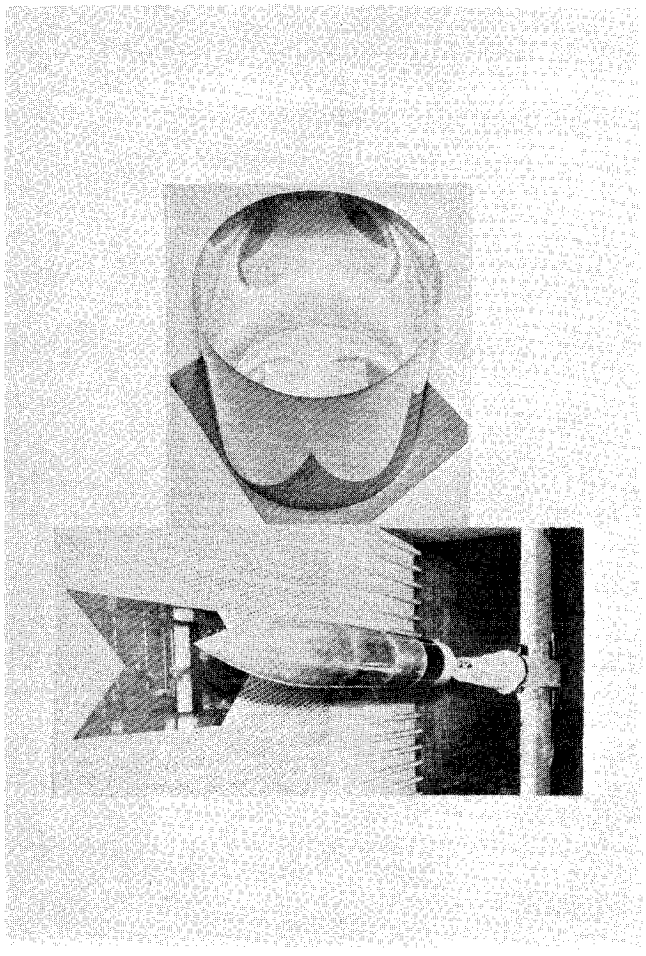

**Fig. 1 Cylindrical shell flutter model and wind-tunnel installation.**

conducive to panel flutter. A reusable launch vehicle or supersonic transport design, however, must impose more stringent restrictions on even the limited amplitude panel flutter occurrences to guarantee vehicle structural integrity over a specified lift time. These considerations and the recent observation of a more highly divergent panel flutter instability on cylindrical shell structures prompted these current experimental studies.[5] The experiments were carried out in the AEDC Propulsion Wind Tunnel Facility over the Mach number range 1.2–3.5. Fourteen different cylindrical shell configurations were studied under different internal stress levels and supersonic flow conditions. All of the shells had a common length to radius ratio of two and radius to thickness ratios from 2000–4000.

## Description of Flutter Model, Instrumentation, and Test Facility

Many parameters influence the panel flutter phenomenon and the realistic scaling of all of these influences is not generally possible in an experiment. Consequently in the present study, the basic geometry of the test shells was maintained as large as possible, compatible with available wind-tunnel facilities. In addition, the shell geometries were taken to be the same as those from a previous large-scale experiment to facilitate a comparison of the present results with these earlier experiments. The facilities of the 16 ft supersonic and transonic Propulsion Wind Tunnel of the Arnold Engineering Development Center proved ideal for the study. These tunnels have a combined Mach number capability ranging from 0.6–4.8 and cover a stagnation pressure range from 60–5000 psf. During the test, the maximum stagnation temperature was held to 200°F, and the Reynolds number ranged from $0.3 \times 10^6$/ft to $6 \times 10^6$/ft. Full details of the wind-tunnel facility and its capabilities are presented in a test facilities handbook available through the Arnold Engineering Development Center.

The experimental flutter model was an ogive cylinder configuration cantilevered at its base from an adjustable length wind-tunnel sting. This basic ogive-cylinder model was chosen because it had been extensively wind-tunnel tested by NASA and many of its aerodynamic characteristics are available.[19–22] The thin shell models under study were circular cylindrical shells fabricated from copper by a special electroforming process and bonded to two heavy copper end rings. A photograph of a typical test shell without end rings, and its installation in the wind tunnel is shown in Fig. 1. The shells were mounted near the base of the ogive cylinder model on the center section structure illustrated in Fig. 2. The electroforming process provided shell models with a high degree of uniformity in both material and geometric properties while minimizing geometric imperfections and initial stresses. In addition, extremely thin shells of $R/h = 4000$ could be easily fabricated in this manner.[24]

The flutter model center section was designed so that an axial compressive force could be applied to the heavy end rings bonded to the shell through two inflatable rubber tubing bladders which when pressurized would bear against the outside face of each ring as illustrated in Fig. 2. The model was supported by two radial bladders which were inflated against the inside diameter of these rings. The radial supporting bladders were also used to effectively seal the annular cavity between the shell and the rigid inner duct so that it could be pressurized. This mounting system was designed to minimize any residual stresses that might result from installation of the thin flutter shells on the ogive cylinder flutter model. The thin shell boundary conditions were thought to closely approximate the fully clamped boundary conditions due to the large cross-sectional dimension of the end ring compared to the shell thickness and to the large mass of the end rings compared to the shell mass.[23]

The center section also supports the displacement measuring instrumentation, and model axial loading and internal pressurization systems. The four displacement sensors, or mutual

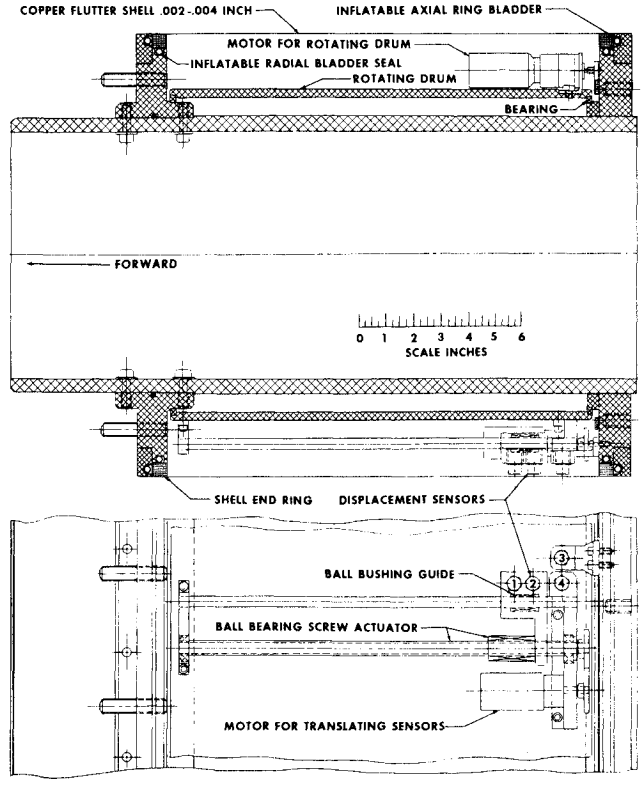


**Fig. 2 Design detail of thin shell supporting structure.**

inductance proximity transduces used to measure both the static and dynamic displacements of the shell surface, are illustrated in Fig. 2. Three of these sensors could be moved relative to a fourth reference sensor through 355° of the shell's circumference. In addition, two of these three sensors could be translated from 10% to 85% of the shell's length. Each sensor position was monitored by a voltage signal from a potentiometer geared to the traversing mechanisms. A correlation of the moving sensor outputs with their position, and with the fixed fourth sensor output permits the discrimination of various possible buckling, vibration, and flutter modes that may occur on the shell.

A boundary-layer control system was installed in the nose cone of the model. It consisted of a circumferential slot through which preheated air or nitrogen could be ejected to trip an existing laminar boundary layer or thicken an already fully developed turbulent profile. The flutter model employed three boundary-layer rakes to measure boundary-layer profiles at several locations over the model surface. Two of the rakes could be remotely positioned over the model surface during the wind-tunnel test. One of these was fixed at the trailing edge of the shell at a given circumferential position but could be moved in a radial direction to accommodate any boundary-layer thickness up to approximately 2 in. A second probe was fixed at a given circumferential position and height but could be moved longitudinally in increments from the boundary-layer control slot in the nose cone to the shell trailing edge. The third rake was fixed at the trailing edge of the shell at a given circumferential position and height. By employing the above instrumentation and control systems the local flow conditions over the shell could be monitored and maintained in the similar form of a fully laminar profile or that of a fully developed turbulent profile.

## Flowfield Study over Flutter Model

During this phase of the program the range of experimental parameters was determined for which flow similarity could be achieved over the center section of the model where the thin flutter shells were mounted for testing. The aeroelastic stability studies were then conducted over this range of parameters to simplify the experimental measurements and the analytical modeling of the problem.

Experiments were conducted to obtain a satisfactory description of the surface pressure distributions over the center section of the flutter model for a sufficiently large range of Mach number, Reynolds number, and boundary-layer control injection rates. This was accomplished by mounting on the ogive model a relatively rigid shell which was instrumented with 24 surface static pressure orifices. The orifices were arranged in four streamwise rows located at 90° circumferential positions as illustrated in Fig. 3. Shell wall or skin temperatures were also measured on this rigid shell through two thermocouples mounted approximately $2\frac{1}{2}$ in. from the ends of the shell at a given circumferential

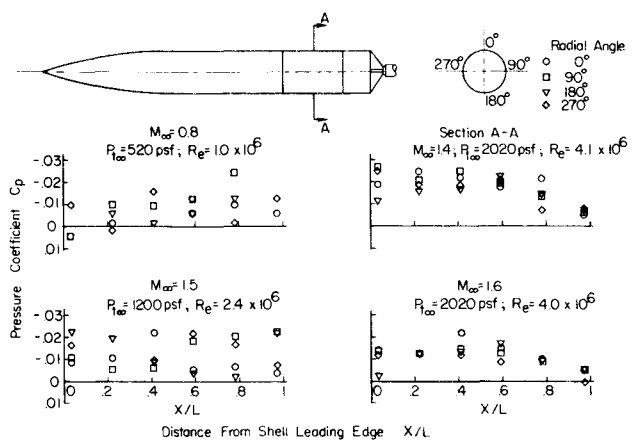


**Fig. 3 Static pressure distribution over test shell in transonic tunnel.**

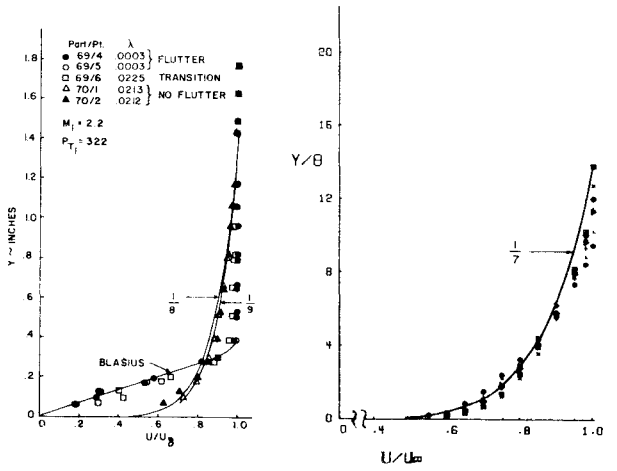


**Fig. 4 Illustration of boundary-layer profiles at flutter occurrences.**

position. Finally, studies were made on the characteristics of the boundary layer over the shell, and on the effectiveness of the boundary-layer control system in changing these characteristics. Boundary-layer profile similarity was investigated by studying velocity profiles, law of the wall, and velocity defect curves computed from measured data. Boundary-layer transition studies were also made over the center section of the flutter model by measuring surface temperature recovery factors, making total pressure surveys along the model axis, and by correlating mean skin-friction coefficients forward of a given model station with the Reynolds number at that station.

Several observations were made concerning the uniformity of the static pressure field over the center section of the flutter model where the thin shells were mounted for testing. When flutter model experiments were conducted in the transonic circuit of the propulsion wind-tunnel facility at Mach numbers above 1.2, the maximum variation in surface static pressure was less than 3% of the freestream dynamic pressure at all operating total pressures or Reynolds numbers. Near the point of model bow shock detachment, which occurred just slightly below Mach number 1.2, the surface static pressure became more nonuniform but again improved at the subsonic Mach numbers. This is illustrated by the data in Fig. 3 taken in the transonic circuit of the wind tunnel. When the model was tested in the supersonic circuit of the wind tunnel, the variations in the surface static pressures were within approximately 1% of the freestream dynamic pressure for all Mach numbers and Reynolds numbers.[12] Mass injection through the boundary-layer control slot did not adversely influence the uniformity of the surface static pressures over the model center section for any of the Mach numbers or Reynolds numbers investigated.

The boundary-layer control system proved quite effective for changing the boundary-layer characteristics over the model center section. In general, both a profile distortion and thickening could be accomplished with the boundary-layer control system on the model. For example, BLC mass injection was observed to trip an existing laminar boundary layer making it thicker and of a fully developed turbulent form over the model center section. This is illustrated by the velocity profile plots in Fig. 4a and the corresponding law of the wall and velocity defect plots illustrated in Figs. 5a and 5b. A representative change in displacement thickness that was accomplished for a similar profile distortion is illustrated in Fig. 6. The boundary-layer thicknesses were at least tripled while the displacement thicknesses were increased by as much as a factor of 10 in these cases. In contrast, profile thickening without profile distortion was accomplished as illustrated in Fig. 4b. This represents a correlation of seven different velocity profiles at three positions over the model center section for different BLC injection rates. Although boundary-layer displacement thicknesses were more than doubled in some

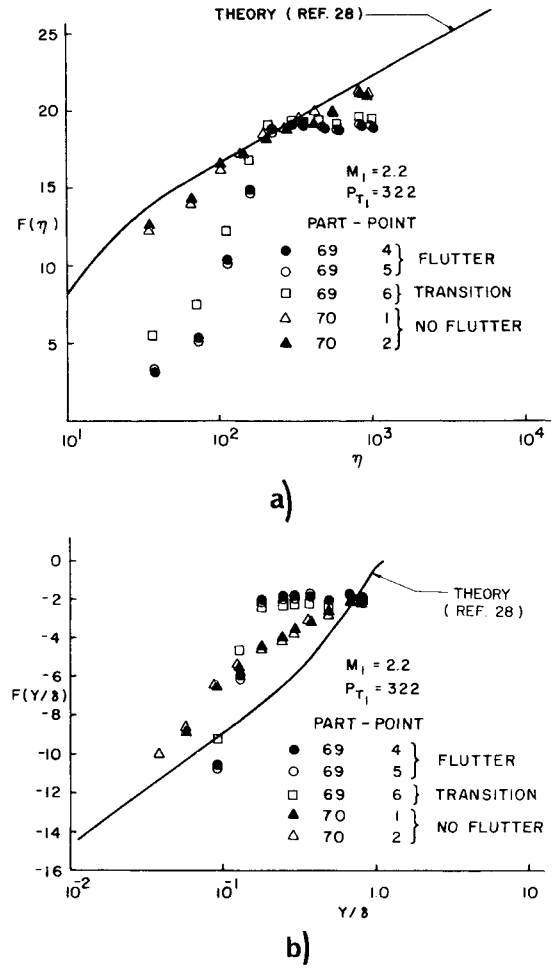


Fig. 5 Law of the wall and velocity defect functions: a) law of the wall; b) velocity defect.

of these cases the velocity profile data all scaled reasonably well when the momentum thickness was employed as a similarity parameter.[25,26] That is, the initially turbulent profiles all retained their fully developed turbulent form although their displacement thickness was more than doubled. Artificial thickening of a laminar profile by BLC activation was not possible since the slightest amount of mass injection would trip the laminar profile creating a fully developed turbulent profile over the model center section.

Laminar profiles could be maintained naturally over the model center section for a given Mach number at the lower Reynolds

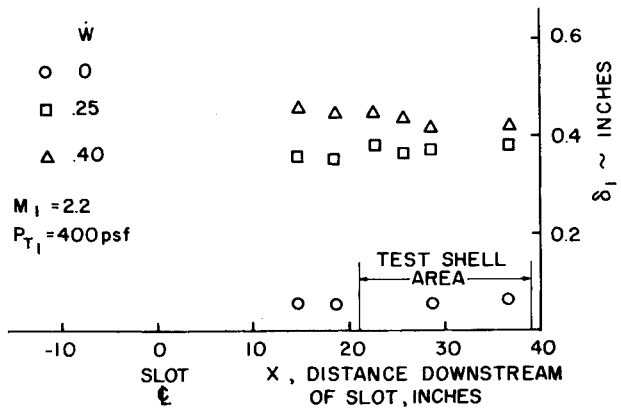


Fig. 6 Variation of displacement thickness over the model for various BLC activation rates.

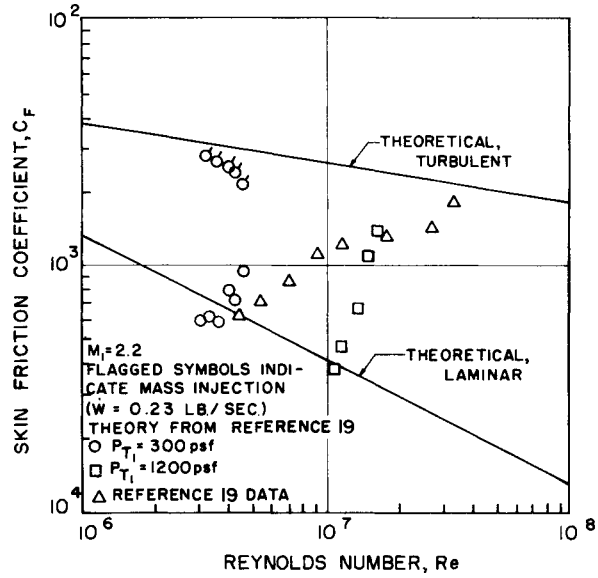


Fig. 7 Variation of mean skin-friction coefficient with Reynolds number.

number flows in the supersonic circuit of the Propulsion Wind Tunnel. A laminar boundary layer, however, could never be established over the model center section for any flow condition in the transonic circuit of the tunnel. Fully developed turbulent profiles and hence similar boundary-layer profiles could be maintained over the model center section for any flow condition or boundary-layer control activation rate in the transonic circuit of the tunnel above Mach number 1.2. In the supersonic circuit of the tunnel, fully developed turbulent profiles could be achieved naturally over the model center section for an operating Reynolds number of $20 \times 10^6$ or above, or for any boundary-layer control activation rate regardless of the Reynolds number. In addition, the temperature recovery factor measurements indicated that the shell surface approximated an adiabatic wall with an average recovery factor of 0.86 for laminar flow and an average factor of 0.89 for turbulent flow.

The transitional characteristic of the ogive cylinder flutter model is illustrated in Fig. 7. This is a correlation of mean skin-friction coefficient up to a certain measuring station on the model with the Reynolds number of the flow at that measuring station. Experimental data from Ref. 19 is presented here along with our measured experimental data. At the lower Reynolds numbers ($P_{T_1} = 300$ psf) our mean skin-friction coefficient data is in agreement with the theoretical laminar curve presented in Ref. 19. When the boundary-layer control system is activated at these lower Reynolds numbers, as indicated by the flagged symbols, the skin-friction coefficients are increased to values approximating the theoretical turbulent skin-friction coefficients. This increase in skin-friction coefficient is attributed to the BLC mass injection artificially tripping the boundary layer and causing the flow to become fully turbulent. At $Re = 1 \times 10^7$, a natural transition is seen to occur on the model for no mass injection. This natural transition is nearly completed at a Reynolds number between $15 \times 10^6$ and $20 \times 10^6$ which is in approximate agreement with the findings of Ref. 19. The slightly higher critical transition Reynolds number observed in this study is attributed to the fact that the present studies were conducted in a much larger wind tunnel than those in Ref. 19.[27]

A comparison between the data reduced according to planar or axial symmetric flow assumptions resulted in no significant differences in the normalized velocity distribution, law of the wall, and velocity defect profiles for boundary-layer thicknesses approximately equal to one-fourth or less of the model's cross-sectional radius. The flow over the center section of the model in all cases appears to be locally two dimensional.

## Observed Shell Instabilities

During the course of the experiments, two basic types of shell instabilities were investigated. This included a buckling or divergence instability both with and without the influence of the supersonic airstream, and a panel fluttering instability. The buckling studies were conducted to determine the influence of the supersonic airstream on the shell buckling loads and to establish a safe shell loading limit for studying panel flutter under combined stress states. The panel flutter studies were conducted primarily to determine the parametric conditions that lead to a highly divergent and catastrophic panel flutter instability in lieu of the more mild limited amplitude instabilities observed in the present and earlier experiments. Several experimental techniques were employed to detect and monitor the onset and basic types of shell instabilities which are discussed below. The basic experimental procedure followed during the course of the study was to maintain wind-tunnel conditions fixed and change the shell model internal stress state or the BLC activation rate to initiate or suppress a shell instability.

## Experimental Definition of Buckling and Flutter

Although the onset of a buckling collapse or highly divergent panel flutter instability was quite evident because of their catastrophic nature, several experimental indicators were employed to distinguish the character of the catastrophic occurrences and to detect the onset of the less violent type of instability. First, the amplitude time histories of different points on the shell's surface were continuously monitored and recorded on magnetic tape during the test along with the applied loading conditions on the shell. On-line visual observation of the shell was also maintained during the testing through closed circuit television monitors. Any interesting observations were recorded visually on high-speed film for later study. Finally, power spectral densities and power spectral distributions were obtained off line for some of the more interesting amplitude time histories by means of a "fast Fourier transform" technique. Any interesting shell response was then classified according to type only after reviewing these different indicators.

### Shell Buckling

The amplitude time history of a point on a shell undergoing a still air buckling collapse under a combined internal pressure and axial compressive load is illustrated in Fig. 8. The final mode of shell collapse is also shown here. Buckling was initiated by preloading the shell under an axial load of 130 lb and an internal pressure of 2 psig. The internal pressure was then slowly decreased, as indicated by the second trace labeled $\bar{p}$, until a buckling collapsed occurred at 0.9 psig. The top trace illustrated the amplitude time history of a point on the shell during this buckling. A small monotonic decrease in the shell radial displacement precedes a large step change in the mean position of the shell which occurs at buckling. The shell again comes to rest in a new equilibrium position having undergone no significant oscillations. Amplitude time histories of a buckling or divergence type collapse of two different shells in the presence of a supersonic flow is illustrated in Figs. 9a and 9b. The shells were loaded under a combined internal pressure and axial compressive force, and divergence or buckling was initiated by slowing reducing model internal pressure while holding flow conditions and other parameters constant. The amplitude time traces for two points on the shell surface are seen to be similar in character to that for still air buckling in that the points on the shell surface essentially jump from one equilibrium position to some final position with no significant oscillations. The amplitude time histories illustrated in Figs. 8 and 9 are taken to be characteristic of buckling or divergence phenomena occurring on the shell.

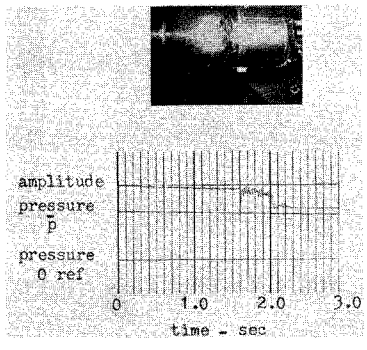


**Fig. 8 Amplitude and model cavity pressure time traces taken during still air buckling of shell under combined internal pressure and axial compressive end loading.**

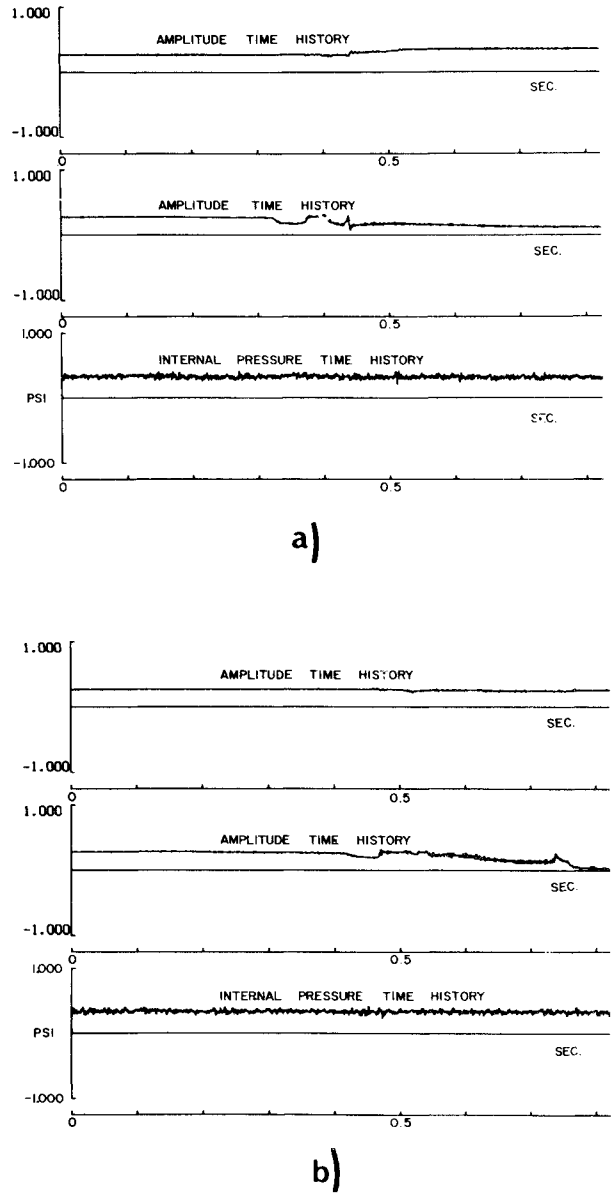


**Fig. 9 Amplitude time and model internal pressure time histories of cylindrical shell buckled under combined internal pressure and axial compressive end load in the presence of a supersonic flowfield, $M_\infty = 2.2$ (motion of two points on shell surface is presented for each event).**

The influence of the supersonic airstream on the buckling characteristics of thin cylindrical shells under combined axial end compressive loading and internal pressure was investigated in Ref. 15 by correlating experimental buckling data from a dozen different test conditions. These included shell buckling studies

**Table 1 Buckling interaction and flutter data**

| Code letter | Event | Source | $M_\infty$ | q psf | $R_\theta$/ft. x $10^{-6}$ | $P_{t_\infty}$ psf | No. times buckled | P lb. | $\bar{p}$ psi | h in. | R/h | $\frac{P}{2\pi Eh^2}$ | $\frac{\bar{p}}{E}\left(\frac{R}{h}\right)^2$ | $2qL^3/\beta D$ x $10^{-6}$ | Boundary layer |
|---|---|---|---|---|---|---|---|---|---|---|---|---|---|---|---|
| a | Buckle | Olson | 3.0 | 425 | | 2474 | 1 | 90 | −0.037 | 0.0040 | 2000 | 0.056 | −0.009 | 0.10 | Laminar |
| b | Buckle | Olson | 3.0 | 545 | | 3173 | 1 | 700 | 3.93 | 0.0039 | 2050 | 0.458 | 1.03 | 0.14 | Laminar |
| c | Buckle | Olson | 0.0 | — | — | — | 1 | 390 | 0.0 | 0.0041 | 1950 | 0.230 | 0.0 | — | Laminar |
| d | Buckle | Olson | 0.0 | — | — | — | 1 | 350 | 0.0 | 0.0040 | 2000 | 0.218 | 0.0 | — | Laminar |
| e | Buckle | Olson | 0.0 | — | — | — | 1 | 400 | 0.0 | 0.0044 | 1820 | 0.205 | 0.0 | — | Laminar |
| f | Buckle | Olson | 0.0 | — | — | — | 1 | 0 | −0.050 | 0.0040 | 2000 | 0.0 | −0.012 | — | Laminar |
| g | Buckle | Jan. '68 | 2.6 | 308 | 1.26 | 1300 | 1 | 200 | 0.111 | 0.0033 | 2420 | 0.250 | 0.047 | 0.16 | Turbulent |
| h | Buckle | Jan. '69 | 2.2 | 111 | 0.50 | 350 | 1 | 200 | 0.055 | 0.0032 | 2500 | 0.222 | 0.025 | 0.08 | Laminar |
| i | Buckle | Jan. '66 | 0.0 | — | — | — | 2 | 130 | 0.900 | 0.0020 | 4000 | 0.406 | 1.03 | — | — |
| j | Flutter | Dec. '56 | 1.2 | 1082 | 5.39 | 2600 | 0 | 0 | 0.240 | 0.0033 | 2420 | 0.0 | 0.100 | 2.01 | Turbulent |
| k | Flutter | Dec. '66 | 1.2 | 1081 | 5.39 | 2600 | 0 | 0 | 0.270 | 0.0031 | 2580 | 0.0 | 0.128 | 2.43 | Turbulent |
| m | Flutter | Dec. '66 | 1.5 | 858 | 4.03 | 2000 | 0 | 130 | 0.910 | 0.0021 | 3800 | 0.334 | 0.940 | 3.68 | Turbulent |
| n | Flutter | Dec. '66 | 1.5 | 857 | 4.02 | 2000 | 0 | 105 | 0.480 | 0.0020 | 4000 | 0.298 | 0.548 | 4.25 | Turbulent |
| p | Flutter | Dec. '66 | 1.2 | 1081 | 5.40 | 2600 | 0 | 210 | 0.520 | 0.0040 | 2000 | 0.169 | 0.148 | 1.13 | Turbulent |
| q | Flutter | Jan. '69 | 2.2 | 313 | 1.47 | 1000 | 0 | 0 | 0.015 | 0.0032 | 2500 | 0.0 | 0.0067 | 0.22 | Turbulent |
| r | Flutter | Jan. '69 | 2.2 | 475 | 1.83 | 1500 | 0 | 0 | 0.060 | 0.0025 | 3220 | 0.0 | 0.045 | 0.44 | Turbulent |
| s | Flutter | Jan. '68 | 2.2 | 102–158 | 0.44–0.72 | 322–500 | 0 | 0 | 3.0–4.2 | 0.0021 | 3880 | 0.0 | 0.91–1.28 | 0.25–0.39 | Laminar |
| t | Flutter–Buckle | Jan. '69 | 2.2 | 313 | 1.47 | 1000 | 1 | 200 | 0.054 | 0.0032 | 2500 | 0.222 | 0.024 | 0.22 | Turbulent |
| u | Buckle | Dec. '66 | | | | | 9 | 240 | 0.0 | 0.0033 | 2420 | 0.250 | 0.0 | | |
| v | Divergence | May '71 | 0.9 | 905 | 5.25 | 2701 | 0 | 0 | 1.43 | 0.0030 | 2500 | 0.0 | 0.638 | 0.308 | Turbulent |
| w | Divergence | May '71 | 0.9 | 905 | 5.28 | 2700 | 0 | 0 | 1.35 | 0.0032 | 2500 | 0.0 | 0.603 | 0.308 | Turbulent |
| x | Divergence | May '71 | 0.9 | 804 | 4.69 | 2400 | 0 | 0 | 0.9 | 0.0027 | 2970 | 0.0 | 0.565 | 0.458 | Turbulent |
| y | Divergence | May '71 | 0.6 | 536 | 4.17 | 2700 | 0 | 200 | 1.5 | 0.0034 | 2360 | 0.196 | 0.594 | 0.0835 | Turbulent |
| z | Buckle | Ames '62 | 2.5 | 272 | 1.48 | 1054 | 2 | 0 | −0.034 | 0.0041 | 1950 | 0.0 | −0.010 | 0.042 | Laminar |
| u' | Buckle (u Second Time) | Dec. '66 | | | | | 9 | 123 | 0.0 | 0.0033 | 2420 | 0.128 | 0.0 | | |

both with and without the influence of an external supersonic flow. The data are presented in Table 1 and on the buckling interaction curve illustrated in Fig. 10. The scale on the pressure axis in Fig. 10 is the same for both positive and negative values. As a result, buckling load points *f, z,* involving only radial pressures lie relatively close to the axially loaded case only, i.e., the origin, because of the small radial buckling pressures of these thin shells. The primary findings here indicate that if the critical loading conditions on a shell under combined axial load and internal pressure cause it to become unstable in a buckling mode at supersonic air speeds then the wealth of existing still air buckling data should be beneficial in estimating the buckling loads of such structures. The influence of the supersonic airstream was found to have no significant effect on the shell's ability to resist a buckling collapse. This requires, of course, that the flow direction be along the axis of the shell, and that no significant cross-flow exists. The data represented by the shaded points in Fig. 10 were taken from still-air buckling tests, while the open symbols represent wind-tunnel test points. The flow conditions and radius-to-thickness ratios of each shell are coded beside each test point (see Table 1). The triangular symbols represent dynamic instabilities (panel flutter), while the remaining open symbols represent static buckling or divergence in the presence of an airstream. The data on this interaction curve indicate that no significant shift occurs in the wind-tunnel buckling load points (open circular symbols) when compared to their still-air buckling counterparts (shaded symbols). The interaction design curve suggested in Ref. 29 constitutes a reasonable design criterion for this static instability. It should be mentioned in passing, that the wind-tunnel buckling studies were conducted under boundary-layer profiles that ranged all the way from a laminar to a fully developed turbulent profile. Nevertheless, no resulting viscous or fluid effects were observed on this buckling type of instability. The buckling mode shapes in the presence of an airstream were also found to be representative of those found in still-air buckling studies. As an illustration, the modal patterns were recorded in detail for the three data points singled out on the buckling interaction curve by the vertical arrows. Proceeding in the direction of increasing model internal pressure, the modal patterns ranged from that of many long shallow elliptic-type buckles equally spaced around the shell circumference for radial pressure loading only, to the classical diamond buckling pattern for combined loading with moderate internal pressures, to the

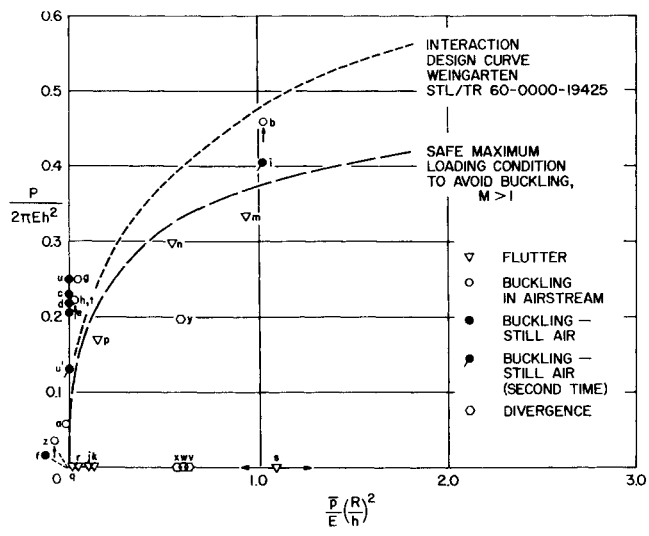


**Fig. 10 Buckling interaction curves and loading conditions on aeroelastically unstable shells.**

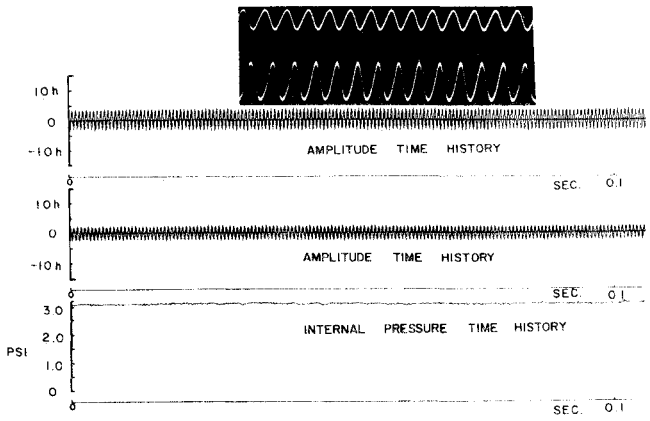


**Fig. 11 Amplitude time and internal pressure time histories of limited amplitude flutter found only in the presence of a laminar or nearly laminar boundary-layer profile (digital and analog traces shown for two points on the surface of the fluttering shell).**

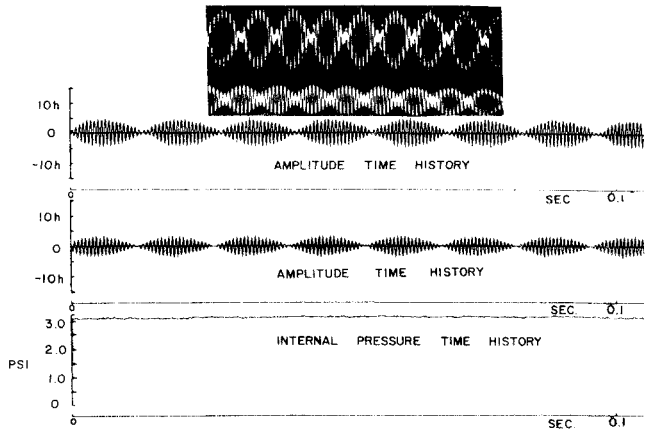


**Fig. 12 Amplitude time and internal pressure time histories of limited amplitude postflutter response found only in the presence of a laminar or nearly laminar boundary-layer profile (digital and analog traces shown for two points on the surface of the fluttering shell).**

fully axially symmetric bellows-type mode for combined loads with high internal pressure levels.[15]

If the critical loading condition on the shell should occur at subsonic Mach numbers, the airstream may have a more significant influence on the buckling phenomena of the shell since the aerodynamic pressure loading tends to be more in phase with the shell deformation. Unfortunately, no satisfactory design criteria or sufficient amount of experimental data, hexagonal symbols, exist which can be used as a guide for estimating the static stability of shells exposed to a subsonic compressible flow.

On the basis of the buckling interaction curve established in Fig. 10 a *maximum safe loading condition* was established that would guarantee a shell safe from buckling or divergence in a supersonic airstream when loaded under a combined internal pressure and axially compressive end loading. This maximum safe loading condition employs, basically, the Weingarten et al. criteria at low values of model cavity pressure and is more conservative than this criteria at the higher values of pressure. This conservative approach is employed because of the lack of experimental data (open symbols) at these higher pressures and to the slightly low single data point observed here. Further experimental studies will probably suggest a design criteria closer to Weingarten et al. curve. According to this maximum safe loading criterion, an unpressurized shell flying at supersonic speeds will have a certain margin of integrity to support axial loads. No negative pressure margin is allowed for these thin shells, however, since small pressure variations in the airstream on the order of 1% of the freestream dynamic pressure could easily induce local buckling of an unpressurized shell because of net inward radial pressure loading only. Although a cylindrical shell should be statically stable for all supersonic flow conditions when loaded under a combined stress state that lies below this curve, it may still be dynamically unstable as indicated by the location of the triangular symbols in the buckling interaction curve of Fig. 10. Finally, as indicated by the hexagonal symbols, a shell under the same still-air loading conditions might also be unstable at the subsonic Mach numbers to an aerodynamic buckling or divergence instability. During the limited experimental study conducted at the subsonic Mach numbers, no panel flutter was observed, but only an aeroelastic divergence.

### Shell Panel Flutter

During the studies associated with cylindrical shell panel flutter, two types of dynamic instabilities were observed. They can be best illustrated by reviewing the character of the amplitude time histories observed at specific points on the shell surface undergoing this motion, and by looking at the related power spectral densities and power spectral distributions of the amplitude time histories. These data are presented in Figs. 11–14, respectively.

One type of motion observed was a nondestructive limited amplitude flutter that occurred in the presence of the laminar boundary layer illustrated in Fig. 4a. The amplitude time traces of two different points on the shell surface during this motion are illustrated in Fig. 11 along with the model internal cavity pressure time history. Both the analog and digitally-plotted

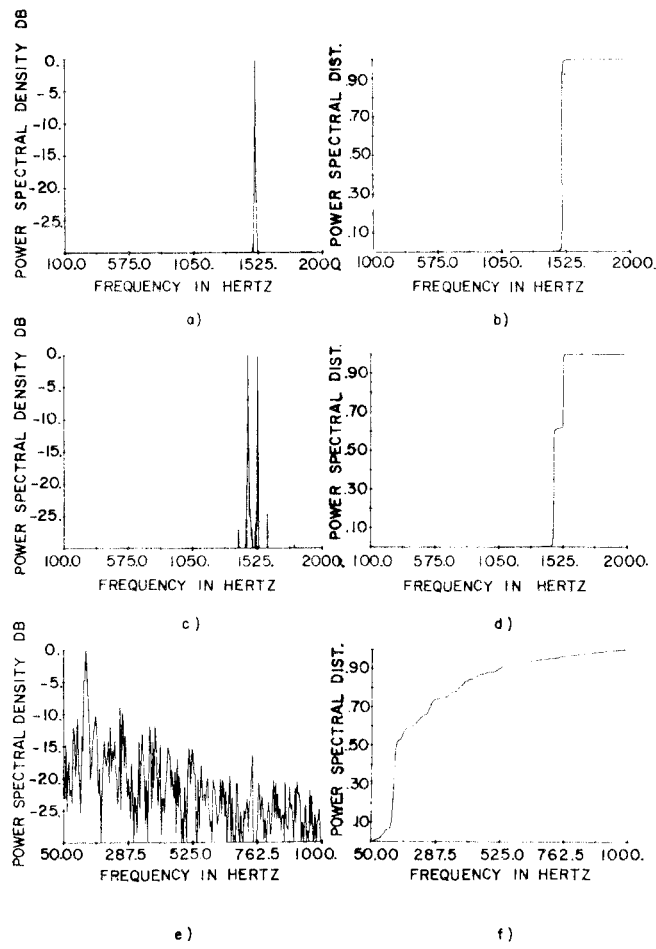


**Fig. 13 Power spectral density and power spectral distribution of flutter occurrences (frequency scale same on all traces).**

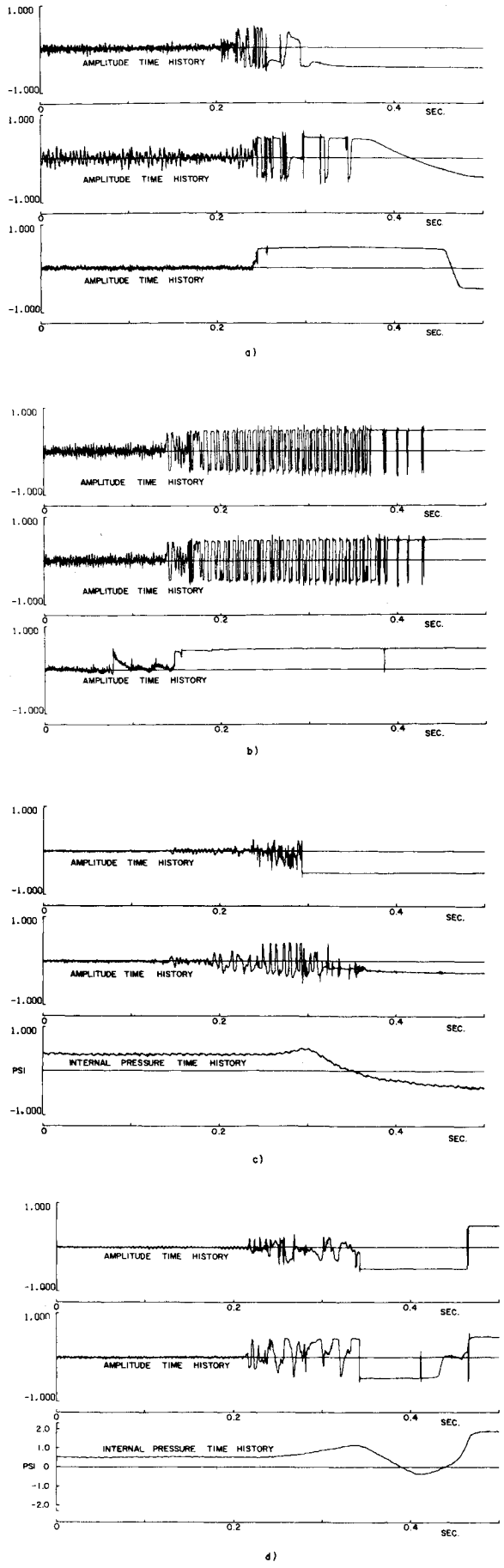


Fig. 14 Amplitude time and pressure time histories of highly divergent flutter found only in the presence of a fully developed turbulent boundary-layer profile.

amplitude time histories are shown illustrating the harmonic character of the motion. The power spectral density, obtained from a fast Fourier transform of the digitized amplitude time histories, is illustrated in Fig. 13a while the power spectral distribution is presented in Fig. 13b. The maximum amplitude of this limited motion was on the order of 4–5 shell thicknesses and the frequency was approximately 1520 cps. The mode shape appeared to be of a standing wave type with many waves around the circumference, but unfortunately a complete description of the mode shape was not obtained. For very small changes in the stress state of the shell or external flow conditions, the amplitude time histories would shift to the form illustrated in Fig. 12. Two modes of the shell appear to be excited in this case as is illustrated by the power spectral density and distribution curves in Figs. 13c and 13d. Motion of the type illustrated in Figs. 11 or 12 was maintained on the shell for approximately $\frac{1}{2}$ hr with no apparent damage to the structure. During this time a range of stress levels and flow conditions were investigated as indicated by the two horizontal arrows associated with the triangular symbol on the buckling interaction curve of Fig. 10. This limited amplitude panel flutter appears similar to that reported earlier in the literature.[1,2,8]

During the course of this experiment it was also observed that the nondestructive limited amplitude flutter could be completely stabilized by tripping the laminar boundary layer making it turbulent and thicker. After this limited amplitude flutter had been sustained on the shell for approximately $\frac{1}{2}$ hr the model BLC system was activated and the boundary-layer profile tipped to the turbulent form illustrated in Fig. 4a. The limited amplitude motion was immediately damped out. It is to be emphasized that the boundary-layer characteristics were the only parameter changes that led to this observation. It was also noticed that no limited amplitude motion of this type was ever observed in the presence of a turbulent profile. Because of the high priority on wind tunnel time, no further investigations on this type of flutter were carried out. Fortunately it was extensively studied in the earlier experiment.[2,8,9]

In contrast to this more mild type of panel instability, a highly divergent flutter motion was observed as illustrated by the amplitude and model cavity internal pressure time histories in Fig. 14. These instabilities occurred in the presence of the fully developed turbulent profile defined by the data in Fig. 5b, and were never observed to occur in the presence of a laminar profile. These highly divergent instabilities were also found to occur at much higher levels of freestream dynamic pressures than the laminar instabilities for a given Mach number. Although the motion in some of these cases appears to be of limited amplitude, this actually represents a saturation of the instrumentation which was not designed to measure shell deformations on the order of an inch or so which occurred during this type motion. In actuality, the highly divergent motion continues to grow until the shell is destroyed to the extent illustrated in Figs. 15a and

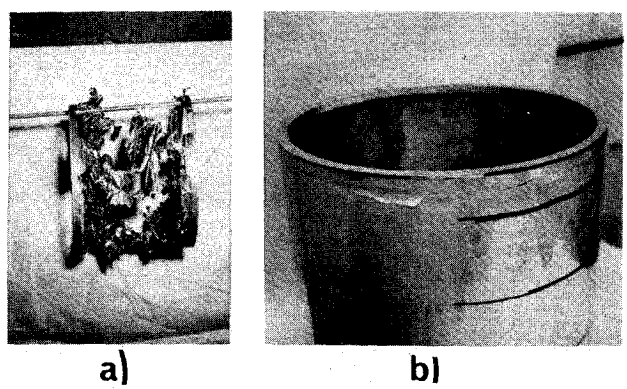


Fig. 15 Illustrations of shell damage induced by highly divergent and catastrophic flutter.

15b. It is apparent from the amplitude time traces that all of the shells were destroyed within less than a second. One exception to this was the shell in Fig. 15b which was destroyed in slightly less than 6 sec. The reason for the longer life span and diminished destruction of this shell was in part attributed to its more rigid inplane constraint in the axial direction because of the use of the end ring locking fixtures. These were not employed for the studies in Fig. 14 or the limited amplitude flutter study. As a result, for the flutter occurrences illustrated in Fig. 14, the amplitude of the shell motion became so large that it finally dislodged the rear ring of these shells forward off its radial bladder support causing their highly excessive destruction as illustrated in Fig. 15a. In spite of the nature of this final failure mode of these shells, it is evident from the high-speed movies taken of these shell failures that the large deformation flutter mode collapsed the shell before the failure of the supporting mount had occurred.

The increased life span of the shell illustrated in Fig. 15b may also be due in part to the actual suppression of this flutter by rapidly pressurizing the model cavity after the onset of flutter. By the time the flutter motion had been suppressed, however, the shell material had been extensively worked by the large amplitude motion and a crack propagated through nearly 270° of the shell circumference in the region where the large amplitude motion occurred near the shell trailing edge. Even though a high air-flow rate into the model cavity managed to sustain a pressure level sufficient to suppress the flutter and maintain the shell shape, its structural integrity was greatly diminished by this large circumferential crack. In essence, the modification in the structural boundary constraint in the axial direction did not seem to alter the character of the highly divergent flutter motion.

In the more catastrophic flutter, the power spectral density curves indicate a wider distribution of energy in the frequency spectrum than that found for the limited amplitude flutter. This is attributed to the fact that the amplitude time traces are so highly divergent that some signal distortion is encountered in these traces because of the saturation of the instrumentation. In these cases the identification of the unstable flutter point in the frequency plane is better identified by the large jump in power illustrated by the power spectral distribution curves.

Our basic findings obtained during this phase of the experimental study indicate that the nature of the boundary layer is an important factor in panel flutter excitation. A laminar or nearly laminar boundary-layer profile was found to induce limited amplitude panel flutter at much lower levels of freestream energy than did a turbulent profile. When panel flutter was observed in the presence of a turbulent profile, however, it was always found to be catastrophic. Finally, it was also observed that panel flutter occurrences at the low freestream energies in the presence of a laminar profile could be suppressed by tripping this profile to a thicker fully developed turbulent form. Once this turbulent boundary layer prevailed over the model, a more catastrophic flutter could be induced, but only at much higher levels of dynamic pressure for a given Mach number.

## Conclusions

The present experimental studies demonstrate that the panel flutter characteristics of thin cylindrical shells are influenced by many parameters which greatly complicate the problem. One important observation, however, demonstrated that the still air buckling characteristics of the shell were not influenced by the supersonic airstream. The wealth of still air buckling design data can consequently be employed to determine the buckling load of cylindrical shells exposed to supersonic airstream. It seems plausible that a subsonic compressible flow may have a more significant influence on the elastic stability characteristics of thin-walled cylindrical shells since in this flow range the pressure distribution tends to be more in phase with the deformation wave form. Unfortunately, no satisfactory design criterion or experimental data exists which can be used as a guide for estimating the static stability of cylindrical shells exposed to a subsonic compressible flowfield. The stability data obtained in the present study are the only information known to the authors for this flow regime.

The viscous fluid boundary layer was found to play an important role in the panel flutter phenomena on thin cylindrical shells. Its influence extends to a higher supersonic Mach number than that found for flat panels.[30] The laminar or nearly laminar boundary-layer profile was found to induce a panel flutter instability at much lower levels of freestream energy than that found for a turbulent profile. When panel flutter occurred in the presence of a turbulent profile, however, it was always found to be highly divergent and catastrophic. During the experimental study it was observed that the limited amplitude flutter, occurring in the presence of a laminar boundary-layer profile, could be completely stabilized by tripping the boundary layer and making it turbulent and thicker. Once this turbulent boundary layer prevailed over the model, a more catastrophic flutter could be induced, but only at much higher levels of dynamic pressure for a given Mach number.

In view of these findings, it is evident that the dynamic aeroelastic modeling of thin shell structures should include the viscous effects in the description of the supersonic flowfield if panel flutter investigations are of interest. This presents an unfortunate complication to the over-all panel flutter problem.

## References

[1] Miles, J. W., Fung, Y. C., and Kaplan, A., "Flutter and Vibration of Pressurized Cylinders," *Transactions of the First Technical Symposium on Ballistic Missiles*, Vol. III: *Aerodynamics and Structures*, Western Development Div., ARDC, and The Ramo-Wooldridge Corp., Los Angeles, Calif., 1956, pp. 71–88.

[2] Stearman, R. O., Lock, M. H., and Fung, Y. C., "Ames Test on the Flutter of Cylindrical Shells," Structural Dynamics Rept. SM 62-37, Dec. 1962, Graduate Aeronautical Labs., California Inst. of Technology, Pasadena, Calif.

[3] Fung, Y. C., "Some Recent Contributions to Panel Flutter Research," *AIAA Journal*, Vol. 1, No. 4, April 1963, pp. 898–909.

[4] Olson, M. D., "Supersonic Flutter of Circular Cylindrical Shells Subjected to Internal Pressure and Axial Compression," Rept. 65-0599, April 1965, Air Force Office of Scientific Research, Wright-Patterson Air Force Base, Ohio.

[5] Stearman, R. O., "An Experimental Study on the Aeroelastic Stability of Thin Cylindrical Shells at the Lower Supersonic Mach Numbers," AFOSR 66-2828 and ARL 67-0006, Dec. 1966, Air Force Office of Scientific Research, Wright-Patterson Air Force Base, Ohio.

[6] Fung, Y. C., "Interaction of Mechanical and Aeroelastic Instabilities of a Circular Cylindrical Shell," *Dynamic Stability of Structures*, Pergamon Press, New York, 1966, pp. 267–284.

[7] Olson, M. D., "Supersonic Flutter of Circular Cylindrical Shells," Ph.D. thesis, May 1966, California Inst. of Technology, Pasadena, Calif.

[8] Olson, M. D. and Fung, Y. C., "Supersonic Flutter of Circular Cylindrical Shells Subjected to Internal Pressure and Axial Compression," *AIAA Journal*, Vol. 4, No. 5, May 1966, pp. 858–864.

[9] Olson, M. D. and Fung, Y. C., "Comparing Theory and Experiment for the Supersonic Flutter of Circular Cylindrical Shells," *AIAA Journal*, Vol. 5, No. 10, Oct. 1967, pp. 1849–1856.

[10] Lemley, C. E., "Design Criteria for the Prediction and Prevention of Panel Flutter," Vols. I and II, AFFDL-TR-67-140, Aug. 1968, McDonnell Douglas Corp., St. Louis, Mo.

[11] Matsuzaki, Y. and Kobayashi, S., "A Theoretical and Experimental Study of Supersonic Panel Flutter of Circular Cylindrical Shells," National Aerospace Laboratory. *Proceedings of the Eighth International Symposium on Space Technology and Science*, Tokyo, 1969, pp. 281–290.

[12] Daily, P., Williams, J., and Stearman, R. O., "Some Recent Experimental Studies on the Aeroelastic Stability of Thin Cylindrical Shells," AFOSR 70-1177TR, Jan. 1970, Air Force Office of Scientific Research, Wright-Patterson Air Force Base, Ohio.

[13] Dowell, E. H., "Panel Flutter—A Review of the Aeroelastic Stability of Plates and Shells," *AIAA Journal*, Vol. 8, No. 3, March 1970, pp. 385–399.

[14] Anderson, W. J. and Hsy, K.-H., "Engineering Estimates for Supersonic Flutter of Curved Shell Segments," *AIAA Journal*, Vol. 8, No. 3, March 1970, pp. 446–451.

[15] Barr, G. W. and Stearman, R. O., "Influence of a Supersonic Flowfield on the Elastic Stability of Cylindrical Shells," *AIAA Journal*, Vol. 8, No. 6, June 1970, pp. 993–1000.

[16] Dixon, S. C. and Hudson, M. L., "Flutter, Vibration, and Buckling of Truncated, Orthotropic Conical Shells with Generalized Elastic Edge Restraint," TN D-5759, July 1970, NASA.

[17] Johns, D. J. and Parthan, S., "Flutter of Circular Cylindrical Shells—A Review," Rept. TT 6917, Nov. 1969, Department of Transport Technology, Loughborough University of Technology, Leicestershire, England.

[18] Leonard, R. W. and Hedgepeth, J. M., "On Panel Flutter and Divergence of Infinitely Long Unstiffened and Ring Stiffened Thin-Walled Circular Cylinders," Rept. 1302, 1957, NACA.

[19] Hilton, J. H., Jr. and Czarnicki, K. R., "An Exploratory Investigation of Skin Friction and Transition on Three Bodies of Revolution at a Mach Number of 1.61," TN 3193, June 1954, NACA.

[20] Czarnecki, K. R. and Monta, W. J., "Boundary Layer Velocity Profiles and Skin Friction Due to Surface Roughness on an Ogive Cylinder at Mach Numbers of 1.61 and 2.01," TN D-2048, Dec. 1963, NASA.

[21] Czarnecki, K. R. and Monta, W. J., "Pressure Distributions and Wave Drag Due to Two-Dimensional Fabrication-Type Surface Roughness on an Ogive Cylinder at Mach Numbers 1.61 and 2.01," TN-D-825, June 1961, NASA.

[22] Czarnecki, K. R. and Monta, W. J., "Roughness Drag Due to Two-Dimensional Fabrication-Type Surface Roughness on an Ogive Cylinder from Force Tests at Transonic Speeds," TN D-5004, Jan. 1969, NASA.

[23] Almroth, B. O., "Influence of Imperfections and Edge Restraint on the Buckling of Axially Compressed Cylinders," CR-432, April 1966, NASA.

[24] Stearman, R. O., "Research on Panel Flutter," AFOSR 65-0247, Dec. 1964, Air Force Office of Scientific Research, Wright-Patterson Air Force Base, Ohio.

[25] Bradfield, W. S., "Research on Laminar and Turbulent Boundary Layers at Supersonic Speeds," AFOSR TR-57-64, Dec. 1957, Air Force Office of Scientific Research, Wright-Patterson Air Force Base, Ohio.

[26] Schlichting, H., *Boundary Layer Theory*, 6th ed., McGraw-Hill, New York, 1968.

[27] Pate, S. R. and Schueler, C. J., "Radiated Aerodynamic Noise Effects on Boundary-Layer Transition in Supersonic and Hypersonic Wind Tunnels," *AIAA Journal*, Vol. 7, No. 3, March 1969, pp. 450–457.

[28] Moore, D. R., "An Experimental Investigation of the Turbulent Boundary Layer Behind a Forward Facing Step in Supersonic Flow," Thesis, June 1958, Defense Research Lab., The University of Texas, Austin, Texas.

[29] Weingarten, V. I. et al., "Final Report on Development of Design Criteria for Elastic Stability of Thin Shell Structures," STL/TR-60-0000-19425, Dec. 1960, Space Technology Labs. Inc.,

[30] Muhlstein, L., Gaspers, P., and Riddle, D., "An Experimental Study of the Influence of the Turbulent Boundary Layer on Panel Flutter," TN D-4486, March 1968, NASA.